Star formation histories of low-mass star forming galaxies at intermediate redshifts[1]

Lucía Rodríguez-Muñoz[1], **Jesús Gallego**[1], **Camilla Pacifici**[2], **Laurence Tresse**[3], **Stéphane Charlot**[4], **Armando Gil de Paz**[1], **Guillermo Barro**[4], **and Víctor Villar**[1]

[1] Dpto. de Astrofísica y CC. de la Atmósfera. Facultad de CC. Físicas, Universidad Complutense de Madrid, Av. Complutense s/n. E-28040, Madrid, Spain
[2] Yonsei University Observatory, Yonsei University, Seoul 120-749, Republic of Korea
[3] Aix Marseille Université, CNRS, LAM (Laboratoire d'Astrophysique de Marseille) UMR 7326, 13388, Marseille, France
[4] UPMC-CNRS, UMR7095, Institut d'Astrophysique de Paris, F-75014 Paris, France
[5] UCO/Lick Observatory and Department of Astronomy and Astrophysics, University of California, Santa Cruz, CA 95064, USA

Abstract

In this work, we present constraints on the star formation histories (SFHs) of a sample of 74 spectroscopically confirmed low-mass star forming galaxies (LMSFGs) with stellar masses $7.3 < \log M_*/\mathrm{M}_\odot < 9.1$ ($\log M_*/\mathrm{M}_\odot \leq 8.0$ for 40% of them), located in the Extended-Chandra Deep Field-South at redshifts between 0.3 and 0.9. We apply a Bayesian approach to fit the spectral energy distributions (including photometry and emission lines measurements) of each galaxy. We use spectral models based on physically motivated star formation (SF) and chemical enrichment histories, and state of the art modeling of the stellar and nebular emission, and dust attenuation. Our work extends the SF Main Sequence over $2\,\mathrm{dex}$ toward lower stellar masses. The median SFH of the sample of LMSFGs shows that more than 90% of the stellar mass estimated for the targets is formed in the $0.7 - 3.0\,\mathrm{Gyr}$ period prior to their observation.

1 Introduction

Low-mass galaxies (here also referred to as dwarf galaxies) are key probes to study galaxy formation and evolution. Their relative simplicity compared to their giant relatives makes

---

[1]Based on observations carried out with the European Southern Observatory (ESO) Very Large Telescope (VLT) at the La Silla Paranal Observatory under programs 088.A-0321 and 090.A-0858.

them unique to identify features of primitive components and the mechanisms of star formation (SF) triggering and quenching. Nevertheless, they are also fragile systems that can be easily disrupted by interactions due to their shallow potential wells. For now, the theoretical studies and models do not agree about their formation and evolutionary scenario (early, e.g., [13]; delayed, e.g., [20]; mass dependent, e.g., [25]). This fact is probably a consequence of the lack of constraints derived from the observation of these systems at different redshifts (and specially outside the local universe), which has been traditionally hampered by the intrinsic low luminosities.

In this work we aim to find observational constraints on the formation and evolution of low-mass galaxies by studying the SFHs of a sample of dwarfs extended over a wide range in redshift.

The work presented here is an extract from the paper [31], accepted for publication in the Astrophysical Journal.

2   Sample and data

To achieve our goal we need to build a sample of candidates to dwarf galaxies at intermediate redshifts on a cosmological field with a deep multiband photometry from UV to near-IR that allows the estimation of photometric redshifts and stellar masses. We use a catalog built on a deep SUBARU NB816 image ([2]) of the Extended-Chandra Deep Field-South (E-CDF-S; [23]) using the Rainbow database[2] ([30, 3, 4]). Rainbow is also a template fitting code based on χ^2 minimization between observed photometry and a set of semi-empirical template SEDs (see [30]). E-CDF-S has available morphology catalogs developed by [17].

We limit our study to the redshift range $0.3 < z_{\mathrm{phot}} < 1.0$ and apparent magnitude $m_{\mathrm{NB816,AB}} < 26\,\mathrm{mag}$ as a balance between the widest redshift range we can reach and the observational limitation, taking into account the follow up spectroscopic confirmation. Then, to identify the final candidates we use two criteria:

- On the one hand, a stellar mass criteria: $\log M_*/\mathrm{M_\odot} < 8$. Such value corresponds also to the range of halo galaxy masses expected to dominate the reionization of cosmic hydrogen ([36]).

- Blue Compact Dwarfs (BCDs; [34]) properties, based on the work by [16]: $M_{\mathrm{B,0,AB}} > -18\,\mathrm{mag}$, $(B - V)_0 < 0.6$, and $S_{\mathrm{R_{eff},B,0}} < 23\,\mathrm{mag\,arcsec^{-2}}$. Among dwarfs, BCDs present observational advantages such as strong emission lines, resulting from the SF burst they undergo, and high surface brightness, which make them excellent tracers of low-mass star forming galaxies (LMSFGs) at intermediate redshifts.

Our final sample of candidates is comprised of ~ 1600 objects (~ 700 selected by mass and ~ 900 selected as BCDs).

---

[2]http://rainbowx.fis.ucm.es

2.1   Photometry

We obtain reliable aperture photometry in 39 different optical and near to medium IR bands across the E-CDF-S field using the Rainbow software package: *Hubble Space Telescope* (*HST*)/Advanced Camera for Surveys (ACS) b, v, i, z bands, and deep VIMOS U and R images from the Great Observatories Origins Deep Survey (GOODS; [15, 27]); the Multiwavelength Survey by Yale-Chile (MUSYC) 18 medium-bands ([7]); HST/Wide Field Camera 3 (WFC3) $F105W$, $F145W$, and $F160W$ from the Cosmic Assembly Near-infrared Deep Extragalactic Legacy Survey (CANDELS; [18, 21]); and in the case of the *Spitzer*/InfraRed Array Camera (IRAC) 3.6, 4.5, 5.8, and 8.0 μm bands, the mean of the value re-measured on the images from GOODS, and those available in the CANDELS-TFIT ([19]) and MUSYC catalogs.

2.2   Spectroscopy

We carry out two programs (088.A-0321 and 090.A-0858) of multi-object spectroscopy using VIsible Multi-Object Spectrograph (VIMOS; [22]), mounted on the 8 m ESO-VLT/UT3 telescope at the La Silla Paranal Observatory (Chile). In total, we observe a subsample of 327 candidates (253 low-mass selected and 74 selected as BCDs). The subsample is selected in order to maximize the number of slits that could be allocated on the masks. Precisely, the masks design is performed with the VIMOS Mask Preparation Software (VMMPS; [5]). We assign a higher priority to the mass-selected sample than to the BCDs.

The two runs use the medium resolution (MR) grism, the associated filter GG475, and 1.2″ and 1.6″ slits respectively. These configurations yield spectral resolutions R $\sim$ 600 and an effective spectral range $4\,800 - 10\,000$ Å. Observations are divided into three VIMOS pointings with total exposure times of 3.3, 2.7 and 3.8 h respectively.

Data are reduced with the VIMOS Interactive Pipeline and Graphical Interface software (VIPGI; [32]) in combination with $\mathrm{R{\small ED}_m^{uce}E}$ software ([8]). VIPGI undertakes standard reducing tasks optimized for VIMOS data including bias subtraction, accurate wavelength calibration ($\sim$ 1Å), identification of objects in the slit, extraction of the one-dimensional spectra, and flux calibration. Figure 1 shows an example of the spectra we obtain.

We then measure accurate spectroscopic redshifts, z_{spec}, with typical uncertainties of $\sim 0.1\%$, for those galaxies that present a minimum of two recognizable spectral features, mainly emission lines given the extremely faint continuum that most of the targets present. We measure redshifts for 94 galaxies out of 327 observed systems, in the range 0.1 to 1.3. The measurements of the emission line fluxes and equivalent widths (EW) are performed using $\mathrm{R{\small ED}_m^{uce}E}$ software ([8]).

In this project we only consider the galaxies for which we find a reliable spectroscopic redshift. For this reason we only include in our study emission line galaxies, and therefore, star forming galaxies. Given the mass range, we are left with a sample of LMSFGs.
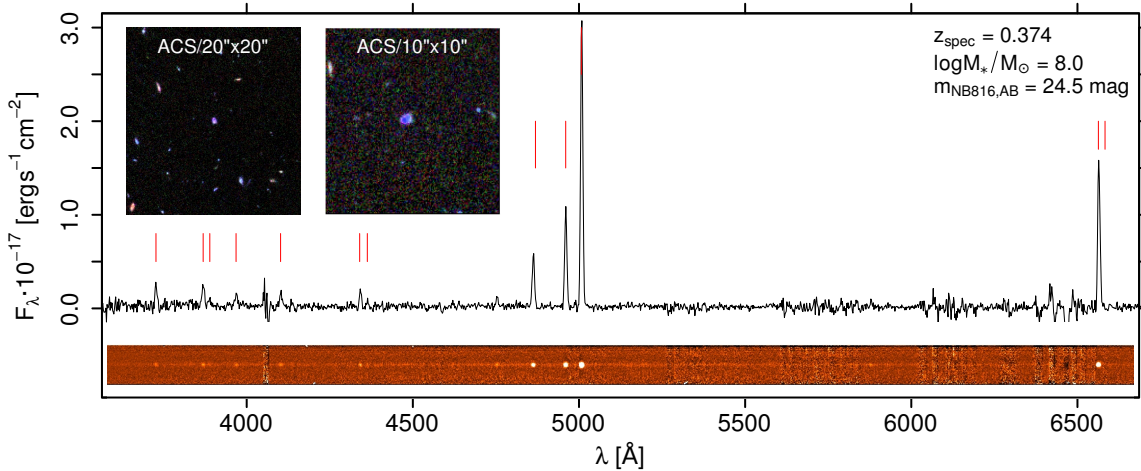
Figure 1: VIMOS spectrum of one of our targets.

3 Modelling and SED-fitting approach

To identify the SFHs of our sample we use the Bayesian approach presented in [28]. We build a large library of physically motivated SF and chemical enrichment histories applying semi-analytic recipes ([12]) to the output of the Millennium cosmological simulation ([33]). Then, we combine this library with state-of-the-art models of stellar population synthesis (latest version of [6]), nebular emission (CLOUDY [14] as in [10]), and attenuation by dust (using [9], as in [29]), in order to build a library of spectral models.

We fit the observational data (photometry and EW of emission lines) to the same observable quantities inferred for the spectral models, and we assign a likelihood to each model (see [28] for the details). Then, we build probability density functions (PDFs) of each physical parameter (stellar mass and SFR) based on the likelihood of the fits. Median values of the PDFs are recorded as the best-estimates of the parameters. The best-estimate SFHs are calculated as the average of the first 10 best-fit model SFHs weighted by their likelihood.

We obtain results for 91 out of 94 galaxies (we dismiss 3 targets for which the approach returns near-zero probability for more than 95% of the models). The 91 galaxies present stellar masses between $6.8 < \log M_*/M_\odot < 9.5$, and SFRs between $-2.8 < \log SFR/M_\odot\ yr^{-1} < 1.0$. Figure 2 (left panel) shows the stellar mass distribution with redshift. We decide to limit our work to the range of redshift approximately homogeneously covered by galaxies in the whole stellar mass range. Targets (74 out of 91) within such redshift range are represented by green points. Blue points show those galaxies outside the range. The central panel in Fig. 2 shows the relation between stellar mass and SFR, also known as the SF Main Sequence (SFMS). Grey contours represent the area populated by SDSS Data Release 7 (DR7; [1]). We find agreement between the relation we obtain for our sample and the SFMS defined by [26] (N07) and [35] (W12).
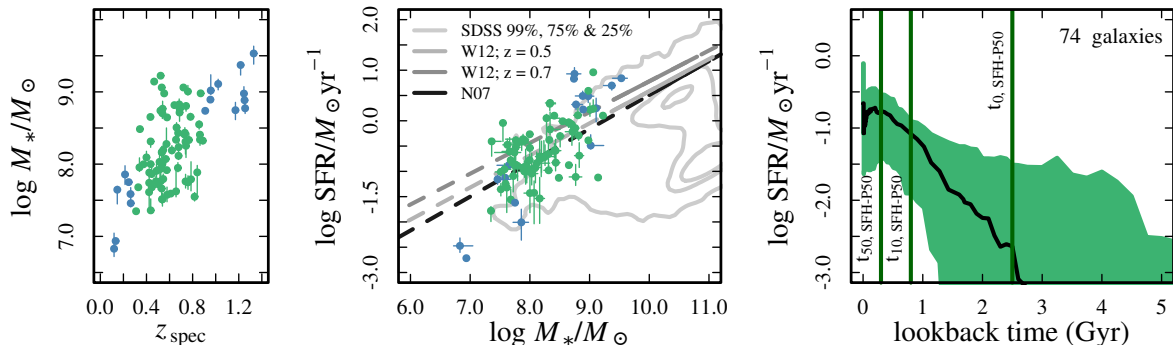
Figure 2: *Left* panel: Stellar mass vs.redshift for our sample of 91 LMSFGs. Galaxies located at redshifts between 0.3 and 0.9 are represented by green points. Blue points mark galaxies outside such redshift range. *Central* panel: Stellar mass–SFR relation. The plot also shows the SFMS found by [35] (W12) for redshifts 0.5 and 0.7 (grey lines) and [26] (N07; black line). We use solid lines to mark the stellar mass ranges within the mass-completeness limits of these studies, and dash lines to extend the SFMSs towards lower stellar masses. In contours we show the distribution of galaxies in the SDSS Data Release 7 (DR7; [1]). *Right* panel: Median SFH (SFH-P50) for our sample of LMSFGs (black solid line). The green area is delimited by SFH-P16 and SFH-P84. The dark green vertical lines mark t_0, t_{10}, and t_{50} for SFH-P50.

4   Star Formation Histories

To characterize the SFHs we calculate the lookback times at which the galaxies ignite the SF (t_0) and form 10% (t_{10}) and 50% (t_{50}) of the final stellar mass.

To identify common behaviors we combine the individual SFHs. First, we normalize the SFHs to the median stellar mass of the sample. Then, we co-add the SFHs previously set to a common reference system where $t_z = 0$. We derive the 50 th, 16 th, and 84 th percentiles of the distribution of SFR at each step in lookback time to build the composite SFH-P50, SFH-P16, and SFH-P84, respectively. Finally, we characterize these SFHs using t_0, t_{10}, and t_{50}, and we estimate their uncertainties using the bootstrapping method. The right panel in Fig. 2 shows SFH-P50 as a black solid line and SFH-P16 and SFH-P84 as the lower and upper limits or the green area. The vertical dark green lines mark the values of t_0, t_{10}, and t_{50} for SFH-P50.

Our sample presents a short median SFH that forms 90% of the median stellar mass ($\log M_*/M_\odot \sim 8.1$) in the $0.7 - 3.0$ Gyr ($t_{10,\mathrm{SFH-P16}}$–$t_{10,\mathrm{SFH-P84}}$) period prior to the observation, and 50% in the last $0.4 - 0.6$ Gyr ($t_{50,\mathrm{SFH-P16}}$–$t_{50,\mathrm{SFH-P84}}$).

The results we obtain when we divide the sample into galaxies with $\log M_*/M_\odot \leq 8.0$ and galaxies with $\log M_*/M_\odot > 8.0$ are very similar for both sub-samples ([31]). Nonetheless, the three milestones (t_0, t_{10}, and t_{50}) tend to be larger for higher mass galaxies.

These results could be interpreted as a sign of the recent stellar-mass assembly of

LMSFGs, in agreement with previous works about SFHs of star forming galaxies (e.g. [24]). Recent formation of low-mass galaxies also matches the downsizing cosmological trend of galaxy formation ([11]). Early SF activity is not dismissed given the large dispersion in $t_{0,\mathrm{SFH-P50}}$ $(1.4 - 6.0\,\mathrm{Gyr})$.

4.1   Conclusions

The main conclusions of our work ([31]) are:

- Our approach locates our sample of LMSFGs on the SFMS and extends it over $2\,\mathrm{dex}$ in stellar mass. The estimated SFRs and stellar masses are consistent with the SFMSs found by [26] and [35].

- The median SFH of our sample of LMSFGs suggests that 90% of the stellar mass is formed in a $0.7 - 3.0\,\mathrm{Gyr}$ $(t_{10,\mathrm{SFH-P16}}$–$t_{10,\mathrm{SFH-P84}})$ period prior to their observation. This result reinforces the view of a recent stellar-mass formation for LMSFGs at intermediate redshifts, which is consistent with the previous work about SFHs of star forming galaxies carried out by [24] and with the downsizing cosmological scenario ([11]).

Acknowledgments

References

[1] Abazajian, K.N., Adelman-McCarthy, J.K., Agüeros, M.A., et al. 2009, ApJS, 182, 543A

[2] Ajiki, M., Mobasher, B., Taniguchi, Y. et al. 2006 ApJ, 638, 596A

[3] Barro, G., Pérez-González, P. G., Gallego, J. et al. 2011, ApJS, 193, 13B

[4] Barro, G., Pérez-González, P. G., Gallego, J. et al. 2011, ApJS, 193, 30B

[5] Bottini, D., Garilli, B., Maccagni, D. et al. 2005, PASP, 117, 996B

[6] Bruzual, G., & Charlot, S. 2003, MNRAS, 344, 1000B

[7] Cardamone, C. N., van Dokkum, P.G., Urry, C. M., et al. 2010, ApJS, 189, 270C

[8] Cardiel, N. 1999 (Thesis)

[9] Charlot, S., & Fall, S. M. 2000, ApJ, 539, 718C

[10] Charlot, S., & Longhetti, M. 2001, MNRAS, 323, 887C

[11] Cowie, L. L., Songaila, A., Hu, E. M., et al. 1996, AJ, 112, 839C

[12] De Lucia, G., & Blaizot, J. 2007, MNRAS, 375, 2D

[13] Dekel, A., & Silk, J. 1986, ApJ, 303, 39D

[14] Ferland, G. J. 1996, University of Kentucky Internal Report, 565 pages

[15] Giavalisco, M., Ferguson, H. C., Koekemoer, A. M., et al. 2004, ApJ, 600L, 93G

[16] Gil de Paz, A., Madore, B. F., & Pevunova, O. 2003, ApJS, 147, 29G

[17] Griffith, R. L., Cooper, M. C., Newman, J. A., et al. 2012, ApJS, 200, 9G

[18] Grogin, N. A., Kocevski, D. D., Faber, S. M., et al. 2011, ApJS, 197, 35G

[19] Guo, Y., Ferguson, H. C., Giavalisco, M., et al. 2013, ApJS, 207, 24G

[20] Kepner, J. V., Babul, A., & Spergel, D. N. 1997, ApJ, 487, 61K

[21] Koekemoer, A. M., Faber, S. M., Ferguson, H. C., et al. 2011, ApJS, 197, 36K

[22] Le Fèvre, O., Saisse, M., Mancini, D., et al. 2003, SPIE, 4841, 1670L

[23] Lehmer, B. D., Brandt, W. N., Alexander, D. M., et al. 2005, ApJS, 161, 21L

[24] Leitner, S. N. 2012, ApJ, 745, 149L

[25] Mamon, G. A., Tweed, D., Thuan, T. X., & Cattaneo, A. 2012, Dwarf Galaxies: Keys to Galaxy Formation and Evolution, 39

[26] Noeske, K. G., Weiner, B. J., Faber, S. M., et al. 2007, ApJ, 660L, 43N

[27] Nonino, M., Dickinson, M., Rosati, P., et al. 2009, ApJS, 183, 244N

[28] Pacifici, C., Charlot, S., Blaizot, J., et al. 2012, MNRAS, 421, 2002P

[29] Pacifici, C., Kassin, S. A., Weiner, B., et al. 2013, ApJ, 762L, 15P

[30] Pérez-González, P. G., Rieke, G. H., Villar, V., et al. 2008, ApJ, 675, 234P

[31] Rodríguez-Muñoz, L., Gallego, J., Pacifici, C., et al. 2014, arXiv1411.0200R

[32] Scodeggio, M., Franzetti, P., Garilli, B., et al. 2005, PASP, 117, 1284S

[33] Springel, V., White, S. D. M., Jenkins, A., et al. 2005, Nature, 435, 629S

[34] Thuan, T. X., & Martin, G. E. 1981, ApJ, 247, 823T

[35] Whitaker, K. E., van Dokkum, P. G., Brammer, G., et al. 2012, ApJ, 754L, 29W

[36] Wyithe, J. S. B., & Loeb, A. 2006, ApJ, 646, 696W